Available online at www.sciencedirect.com
ScienceDirect
Journal of the European Ceramic Society 31 (2011) 1753–1761
www.elsevier.com/locate/jeurceramsoc

Formation and characterization of three-ply structured multiferroic $Sm_{0.88}Nd_{0.12}Fe_{1.93}$–$Pb(Zr_{0.53}Ti_{0.47})O_3$ ceramic composites via a solid solution process

Hongfang Zhang [a,*], Siu Wing Or [a], Helen Lai Wa Chan [b], Fang Yang [a]

[a] *Department of Electrical Engineering, The Hong Kong Polytechnic University, Hung Hom, Kowloon, Hong Kong*
[b] *Department of Applied Physics, The Hong Kong Polytechnic University, Hung Hom, Kowloon, Hong Kong*

Received 20 October 2010; received in revised form 8 March 2011; accepted 17 March 2011
Available online 12 April 2011

Abstract

A new three-ply structured multiferroic $Sm_{0.88}Nd_{0.12}Fe_{1.93}$–$Pb(Zr_{0.53}Ti_{0.47})O_3$ (MS-PZT) ceramic composite has been developed successfully by cofiring at 900 °C under argon atmosphere via a solid solution process. The magnetic and polarization hysteresis loops prove the coexistence of the ferromagnetic and ferroelectric phases in the composites. TEM images show the alloy particles were dispersed uniformly and mainly located at the PZT grain boundaries. The DC resistivity as high as 10^9–10^{10} Ω.cm was obtained and only varies slightly with the volume fraction of the conductive phase $Sm_{0.88}Nd_{0.12}Fe_{1.93}$. The composites can be poled under a high electric field strength at a temperature of 150–180 °C. The dielectric, piezoelectric, and magnetic properties of the composites can be tailored according to the desirable requirement to meet designated application by a simple, flexible, and reproducible route, providing a promising potential approach to a new class of electric circuit and significant miniaturization of devices.

Keywords: Powders-solid state reaction; Composites; Electrical properties; Piezoelectric properties; Three-ply-structure

1. Introduction

Multiferroic materials combining two or more primary ferroic order parameters (ferroelectricity, ferromagnetism and ferroelasticity) [1] have attracted considerable research activity in recent years.[2–8] Ferromagnetic and ferroelectric multiferroics are particularly appealing not only because they have the properties of both parent compounds, but also because interactions between the magnetic and electric polarizations lead to their multifunctionality.[9] As well known, the coupling interaction between ferroelectric and ferromagnetic substances could produce an interesting effect: the magnetoelectric (ME) effect, which is characterized by an induced electric polarization in a material upon the application of a magnetic field, or by an induced magnetization in a material upon the application of an electric field.[10] Magnetoelectric materials are potentially useful in magnetic field sensors and magnetoelectric transducers due to their intrinsic effect upon the conversion between magnetic and electric signals without the aid of any external sources of power.[11] Importantly, following the general tendency of the microelectronic industry towards miniaturizaton and integration, finding materials with best properties in smaller volumes and combining more than one function in the same structure has become highly desirable. However, natural multiferroic single-phase compounds are rare, and their magnetoelectric responses are either relatively weak or occurs at temperatures too low for practical applications (i.e. ∼0.02 V/cm.Oe for Cr_2O_3).[12] The breakthrough in terms of the giant magnetoelectric effect was achieved in composite materials, in which the ME effect is realized in composites on the concept of product property.[13] According to this principle, a suitable combination of two phases such as magnetostrictive and piezoelectric phases, can yield a desirable ME property. For example, the multilayer structures [i.e. ferrite/lead zirconate titanate (PZT),

* Corresponding author. Tel.: +852 2766 6690; fax: +852 2330 1544.
E-mail address: zhf057@gmail.com (H. Zhang).

0955-2219/$ – see front matter © 2011 Elsevier Ltd. All rights reserved.
doi:10.1016/j.jeurceramsoc.2011.03.032

Terfenol-D/PZT, and Terfenol-D/$Pb(Mg_{1/3}Nb_{2/3})O_3$–$PbTiO_3$ etc.] [14–18]; co-sintering particulate composites [such as cobalt ferrite (CFO)/barium titanium ($BaTiO_3$), nickel ferrite (NFO)/$BaTiO_3$ etc.] with 0–3 connectivity patterns [19–21]; and column-structure composites [i.e. Terfenol-D/Epoxy and single PZT rods] with 1–3 connectivity patterns [22] are reported to possess an increased magnetoelectric effect of 3–230 times that in single-phase materials. The challenges of laminated composites include the high eddy-current losses, high mechanical brittleness and weak mechanical coefficients of the constituents. Suitable size and dimensional designs are essential to the applications in electric current sensors at high frequency and in micro-ME devices. In 0–3 particulate ceramic composites, atomic interfacial diffusion and/or reaction problems between the two ceramic phases during high-temperature preparation will deteriorate the predicted properties.[15] While in 1–3 type composites containing Terfenol-D/Epoxy and single PZT rods, good interfacial contact and low resistivity of Terfenol-D are two issues.

In the present work, inspired by building materials "three-ply wood", we have successfully developed a new three-ply structured multiferroic ferromagnetic-ferroelectric ceramic composite by a conventional solid solution process. In this novel structure, in order to reduce the eddy current losses, finer-grained magnetostrictive $Sm_{0.88}Nd_{0.12}Fe_{1.93}$ (denoted as MS) powders are dispersed into micro-sized $Pb(Zr_{0.53}Ti_{0.47})O_3$ (PZT) powders thoroughly to form a homogeneous 0–3 connectivity pattern as the interlayer. Then, layers formed by the glass-coated nano-sized PZT are applied onto the two sides of the interlayer as the insulating layers to solve the leakage current problem. Subsequently, the pellets are pressed and cofired at 900 °C in argon for 4 h. A dense, smooth, and flat three-ply structured ceramic composite (similar to the three-ply wood) was obtained with good interfacial contacts between layers.

To the best of our knowledge, this is the first report on multiferroic ceramic composites combining magnetostrictive alloy and ferroelectric materials cofired by the conventional ceramics processing, and the composites have excellent sum properties of the parent phases. For example, one advantage of the new structure is cofiring at a low sintering temperature of 900 °C, avoiding the use of polymer binder. A magnetoelectric coupling could be achieved [23] without voltage loss induced in the interlayer. Moreover, bulk ceramic composites are desirable over layered samples due to superior mechanical strength.[24] The geometric configurations and dimensions can be tailored to suit specific design requirements. One could also easily control the dielectric, magnetic, electrical and ME parameters with proper choice in the two phases and their volume fractions, presenting a simple, flexible and reproducible process. Also, it is interesting to find that a DC resistivity as high as 10^9–10^{10} Ω.cm was obtained despite the composites contain various volume fraction of the conductive phase ($Sm_{0.88}Nd_{0.12}Fe_{1.93}$). Finally, the new three-ply structure provides a promising potential of using the cross-correlation between the magnetic and electric properties in electronic devices. The processing route, sintering behavior and microstructures, dielectric and magnetic properties, and piezoelectricity are presented in more details in the following Sections.

2. Experimental procedure

2.1. Processing route for preparing the three-ply structured ceramic composites

2.1.1. Preparation of glass-coated nano-sized PZT powders by a modified hybrid process

In this work, a modified hybrid process is introduced to prepare glass-coated nano-sized PZT powders. Firstly, nano-sized polycrystalline PZT powders were prepared by a sol-gel method using a polymer-assisted polyvinylpyrrolidone (PVP- K30 with number-average molecular weight of 10,000). PZT sol precursor was prepared from solutions of molar compositions, $Pb(CH_3COO)_2$:$Zr[CH_3C(O)CHC(O)CH_3]_4$:$Ti(OC_4H_9)_4$:PVP:$C_3H_7{}^iOH$ = 1:0.53:0.47:1:20, where moles of PVP represent those of the monomer (polymerizing repeating unit) of PVP. The concentration of the PZT sol precursor is 0.4 M. The PZT sol was dried at 120 °C for 10 h, resulting in a dried gel-PVP precursor. The gel was heat treated in a muffle furnace and single phase PZT nano-sized powders were obtained at 800 °C for 2 h. Secondly, in this investigation, PbO–B_2O_3–SiO_2 (PBS) ternary phase with the molar ratio of 40:40:20 is selected and used in the crystallization of $Pb(Zr,Ti)O_3$. The concentration of the PBS glass solution was adjusted to 1 M, 100 ml with the solvent ethanol. Then, the solution was poured into glass vessel and covered for three days at room temperature to form a gel. The translucent gel was dried at a temperature of 120 °C for 10 h for further processes.

Finally, the nano-sized PZT powders were dispersed into the PBS gel solution dissolved in solvent ethanol (instead of PBS sol precursor), and mixed thoroughly to form PZT-PBS powder-solution suspension/slurry by conventional ball milling for 2 h. The mass ratio of the PBS gel powders to the nano-sized PZT particles was 5 wt% to give a balance between the processing behavior and properties of the resulting ceramics. The as-prepared uniformly distributed PZT-PBS slurry was dried at 120 °C, calcined at 450 °C for 2 h, and granulated to obtain the glass coated nano-sized PZT ceramic powders which subsequently can be sintered at low temperature.

2.1.2. Formation of the new three-ply structured ceramic composites

The schematic illustration of processing procedure of the three-ply structured ceramic composites is shown in Fig. 1. First of all, finer-sized magnetostrictive $Sm_{0.88}Nd_{0.12}Fe_{1.93}$ (Shenyang National Laboratory for Materials Science, Chinese Academy of Sciences) powders were prepared by a high-energy planetary ball-milling machine (Frisch Pulverisette 5) with stainless milling jar and tungsten carbide milling medium, a solvent ethanol was employed during the ball milling course. Next, the finer-sized MS particles (as the filler) were well dispersed into the granulated commercial micro-sized PZT (53/47) (APC-850, American Piezoceramics, Inc., PA) powders (as the matrix),

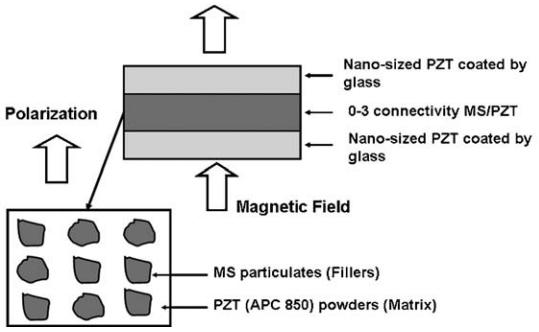

Fig. 1. Schematic diagram of the fabrication of three-ply-structured multiferroic ceramic composites.

and formed the 0–3 connectivity pattern as an interlayer of the three-ply structure. Then, layers formed by the glass-coated nano-sized PZT powders were applied onto the two sides of the interlayer as insulating layers. The mass ratio of MS particles to PZT powders is defined in Eq. (1):

$$W_{\mathrm{MS}}(\mathrm{wt\%}) = \frac{W_{\mathrm{MS}}}{W_{\mathrm{PZT_{Total}}}} \times 100\%, \quad W_{\mathrm{PZT_{Total}}} = W_{\mathrm{PZT_{layers}}} + W_{\mathrm{PZT_{interlayer}}} \quad (1)$$

That is, for the interlayer MS-PZT, the MS content shown in Eq. (1) is equal to Eq. (2):

$$W_{\mathrm{MS}}(\mathrm{wt\%}) = \frac{W_{\mathrm{MS}}}{W_{\mathrm{PZT_{interlayer}}} + W_{\mathrm{MS}}} \times 100\% \quad (2)$$

Here, W_{MS} is the weight of $Sm_{0.88}Nd_{0.12}Fe_{1.93}$ particles; $W_{\mathrm{PZT_{Total}}}$ denotes the total weight of PZT powders used in the structure, and $W_{\mathrm{PZT_{layers}}}$ is the total weight of PZT powders used in the top and bottom insulating layers, $W_{\mathrm{PZT_{interlayer}}}$ is the weight of PZT (APC-850) powders forming the interlayer. Three-ply structured composites with various W_{MS}(wt%) compositions: 1 wt% [for the interlayer $W_{\mathrm{PZT_{interlayer}}}$, the MS content is equal to 2.4 wt% (1.87% volume fraction of MS content)], 3 wt% [for $W_{\mathrm{PZT_{interlayer}}}$, that is equal to 7.5 wt% (7.03 vol%)], 5 wt% [for $W_{\mathrm{PZT_{interlayer}}}$, that is equal to 11.62 wt% (10.69 vol%)], 7 wt% [for $W_{\mathrm{PZT_{interlayer}}}$, that is equal to 15.82 wt% (14.69 vol%)], and 10 wt% [for $W_{\mathrm{PZT_{interlayer}}}$, that is equal to 21.73 wt% (20.16 vol%)], have been investigated in the present experiment. Briefly, the MS content is denoted as 1 ∼10 wt% discussed as follows.

Finally, the powders composed of the interlayer, insulating layers, were uniaxially pressed into pellets with a diameter of 13 mm and a thickness of 1–2 mm at a pressure of 4 MPa in a stainless steel die. The pressed pellets were cofired at 900 °C under argon atmosphere for 4 h.

The process route is simple, flexible, reproducible, and can be applied to synthesize different ceramic materials varying from single-phase ceramics to multiphase ceramics, depending on how the insulating layers (i.e. PZT) are combined with the interlayer with low resistivity (i.e. highly conductive alloy particles). In addition, to solve the thermal expansion mismatch during the sintering process is a key factor to produce a dense, smooth, and flat ceramic material. Owing to the cofiring via the solid solution process, the three-structures (three layers: insulting layers and interlayer) can be adjusted to meet the various design requirements, such as capacitance, piezoelectricity, or ferromagnetism and so on. Moreover, as to the three-structures, combining the merits of the two technologies: the insulating layers with a finer grain size of composition by a modified hybrid process; while the well crystallized powders as the interlayer contributing to the good physical properties, can be expected to produce high-performance ceramics at low sintering temperatures.

2.2. Property measurements

The phase composition of the powders and the composites was examined by X-ray diffraction (XRD, Philips X'Pert-Pro MPD) with CuKα1 radiation (1.5406 Å, 40 kV, 30 mA) at scan step of 0.05° under room temperature. The morphology of the composites and powder was observed by field emission scanning electron microscopy (SEM, JEOL JSM-6335F) and transmission electron microscopy (TEM, Philips CM20) working at 200 kV, respectively. The elemental analysis was done by energy dispersive X-ray spectroscopy (EDS) during the SEM and TEM measurements. Magnetization measurements were performed on a vibrating sample magnetometer (VSM, Lakeshore 7300 series, USA) at room temperature.

To study the dielectric and piezoelectric behaviors, low temperature silver paste was applied onto both sides of the ceramic composites, and heat treated at 600 °C for 30 min to form silver electrodes. The dielectric spectrum was measured with an Agilent 4294A impedance analyzer. The DC resistivity was acquired using an electrometer (Keithley 6517A) at room temperature.

The polarization–electric field (P–E) hysteresis loop measurements for the composite ceramics were carried out using a modified Sawyer Tower circuit at a frequency of 100 Hz at room temperature. The piezoelectric constant d_{33} was measured by a standard piezo d_{33} meter.

3. Results and discussion

3.1. Sintering behavior and microstructure

Fig. 2 shows the X-ray diffraction (XRD) patterns: (a) the commercial micro-sized PZT (APC 850) powders, (b) the nano-sized PZT powder sintered at 800 °C for 2 h in air, (c) and (d) the glass-coated nano-sized PZT powders sintered at 800–000 °C for 2 h in argon, respectively, (e) the finer-sized $Sm_{0.88}Nd_{0.12}Fe_{1.93}$ powders, together with (f) a typical three-ply structured ceramic composite with 5 wt% MS content sintered at 900 °C in argon.

As shown in Fig. 2(a), the XRD pattern indicates the presence of highly crystalline perovskite structure in commercial PZT powders, showing the micro-sized PZT is in a tetragonal phase. The XRD pattern in Fig. 2(b) exhibits a pure perovskite phase in the nano-sized PZT powders prepared by the polymer-assistant sol–gel technique. While, in Fig. 2(c) and (d) of the glass-coated nano-sized PZT powders, all the PZT peaks are identified with no detection of intermediate or interfacial phases. The results indicate the success in synthesizing low temperature sintering nano-sized PZT powders coated by glass using the modified hybrid processing route.

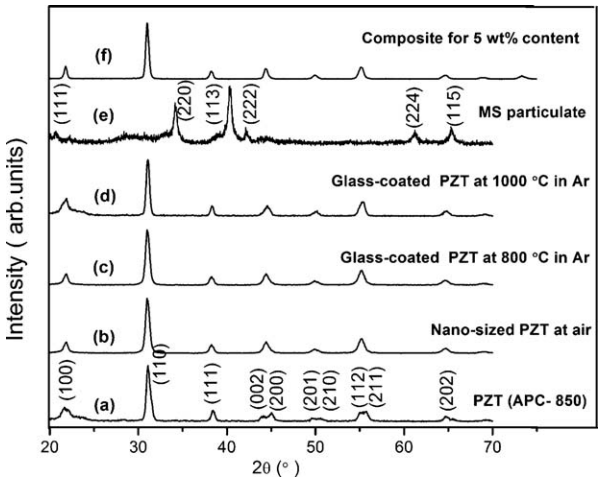

Fig. 2. The X-ray diffraction (XRD) patterns: (a) the commercial micro-sized PZT (APC 850) powders, (b) the nano-sized PZT powder by sol–gel technique sintering at 800 °C for 2 h in air, (c) and (d) the glass-coated nano-sized PZT powders sintered at 800–1000 °C for 2 h in argon, respectively, (e) the finer-grained $Sm_{0.88}Nd_{0.12}Fe_{1.93}$ powders, together with (f) the typical three-ply structured ceramic composite for 5 wt% MS content sintered at 900 °C in argon.

In Fig. 2(e), all the peaks are consistent with those of polycrystalline $Sm_{1-x}Nd_xFe_{1.93}$ ($x = 0$–0.36) compounds, which can be fitted by a profile by assuming a cubic $MgCu_2$-type Laves phase structure. [25] As shown in Fig. 2(f), the XRD pattern of composite ceramics does not show the peak of the $Sm_{0.88}Nd_{0.12}Fe_{1.93}$ phase. This may be due to two main reasons, one is because the thickness of the PZT insulating layers is between 0.3 and 0.5 mm, the intensity of the XRD cannot penetrate the insulators (usually below 40 μm). The other is the scan step at 0.05° which is too fast to detect the minute-phase due to the sensitivity of XRD used at present. However, the ferromagnetic phase ($Sm_{0.88}Nd_{0.12}Fe_{1.93}$) coexisting with PZT in the three-ply structured composites can be proved and confirmed by using the TEM, EDS analysis and magnetic property (magnetic-hysteresis loops) measurement presented in the following sections, respectively.

Fig. 3(a) shows the photograph of a typical three-ply structured composite with 5 wt% MS content sintered at 900 °C for 4 h; (b) and (c) show the highly magnified cross-sectional images of the insulating layer and interlayer, respectively. In Fig. 3(a), a smooth and flat surface was observed with a well-controlled three layers. In Fig. 3(b), a dense, well-developed, and fine-grain PZT phase (~0.5 μm in size) was uniformly dispersed in the glass matrix sintered at 900 °C using the modified hybrid process, forming as the PZT insulating layer. The EDS analysis (not shown) indicated that the composition of the crystal grain was only Pb, Ti, Zr and O element, and the Si element appears in the grain boundary. However, in Fig. 3(c), it is difficult to distinguish $Sm_{0.88}Nd_{0.12}Fe_{1.93}$ particles from the PZT matrix (~1 μm in size).

Fig. 4(a)–(e) show the TEM micrographs together with elemental analysis used to analyze the metal particle distribution in the interlayer of the composite in Fig. 3(c). To keep the original morphology of the composite, the TEM specimens were prepared by depositing the particles (scraping the surface of the interlayer) onto a TEM copper grid coated with lacey carbon, and then ethanol solution was sprayed on the deposited particles, and dried in air. In Fig. 4(a) and (b), fine MS particles (marked with grain number 1 and 2 about 200 nm and 3–5 about 50–500 nm in size, respectively) are mainly located at the PZT grain boundaries. The EDS analysis shown in Fig. 4(c)–(e) reveals the marked grain number 1–5 is the Fe-containing $Sm_{0.88}Nd_{0.12}Fe_{1.93}$ phase (the other elements will be confirmed by following EDS analysis during the FE-SEM measurement), and the grain number 6–7 is the composition of PZT phase element, respectively. For the MS alloy powders, the particle size distribution was approximately 50–500 nm, which is characteristic of the high-energy ball-milling technique. [26] Also, the highly interfacial contact between the bi-phase particles is observed in the interlayer.

We also investigate the element distribution in the three-structures. Fig. 5(a) shows the typical backscattering of the fractured surface of the composite for 5 wt% MS content (a broken sample was selected for examination); and Fig. 5(b) shows the EDS analysis of the marked district (spectrum 3) in the interlayer. Fig. 5(c) displays the elemental analysis curve of the marked districts in Fig. 5(a), which proves the coexistence of magnetic alloy elements and ferroelectric phase elements simultaneously in the interlayer.

The hybrid process has been developed by us in previous reports. [20,21,27–28] The main feature is to combine the merits of high crystallinity and high performance of nanocrystalline particles with those of low sintering temperature such as the sol–gel wet chemistry process, and it is easy to achieve a modification of the processing behaviors of ceramics, which is useful to produce fine-grained and high-performance ceramics at low sintering temperatures.

It is well known that it is difficult to fabricate particulate composite ceramics combining with the conductive magnetostrictive alloy and PZT powders by the conventional ceramic process. This is because the stress developed during the sintering and cooling processes causes large expansion and contraction, and metal usually has a much higher thermal expansion coefficient than the ceramics.[29] Therefore, thermal expansion compatibility is a big challenge for preparation of this new structure by cofiring. Fractured and cracked surfaces of the composite would easily occur. In this work, we successfully get over the difficulties attributing to the flexible process used. For example, different grain sizes have been selected and used in the new structure. As for the insulating layers, nano-sized PZT powders are used, and for the interlayer, the micro-sized PZT powders (APC-850) are selected. A modified hybrid process is introduced to produce the low sintering temperature PZT glass-ceramic keeping the highly crystalline PZT phase content, which is one merit of the process. Therefore, during the cooling process, these achievements can ease the trouble of thermal expansion coefficient efficiently, and a well-developed composite with dense, smooth, and flat surface is obtained. Lastly, the low sintering temperature of 900 °C can suppress metal $Sm_{0.88}Nd_{0.12}Fe_{1.93}$ particles diffusion, mitigate the elements Pb, and Sm evaporation, and retard the chemical reaction between the constituents, which ensures the

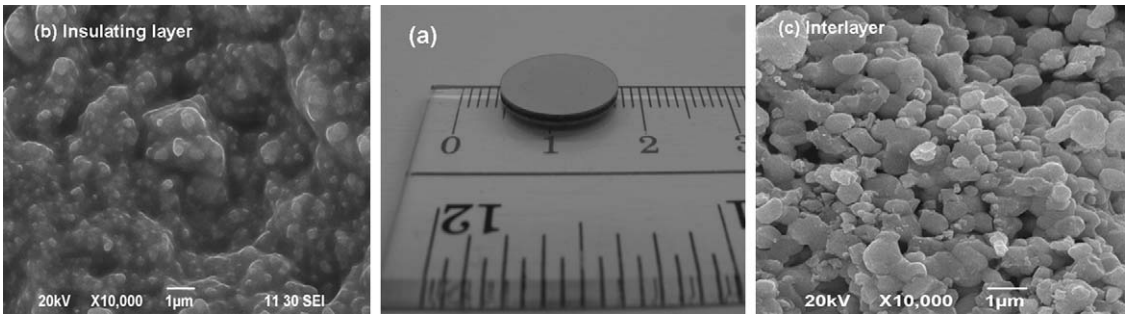

Fig. 3. (a) Photograph of the typical three-ply structured composite with 5 wt% MS content sintered at 900 °C for 4 h, and (b) and (c) show the highly magnified cross-sectional SEM micrographs of the insulating layer and interlayer, respectively.

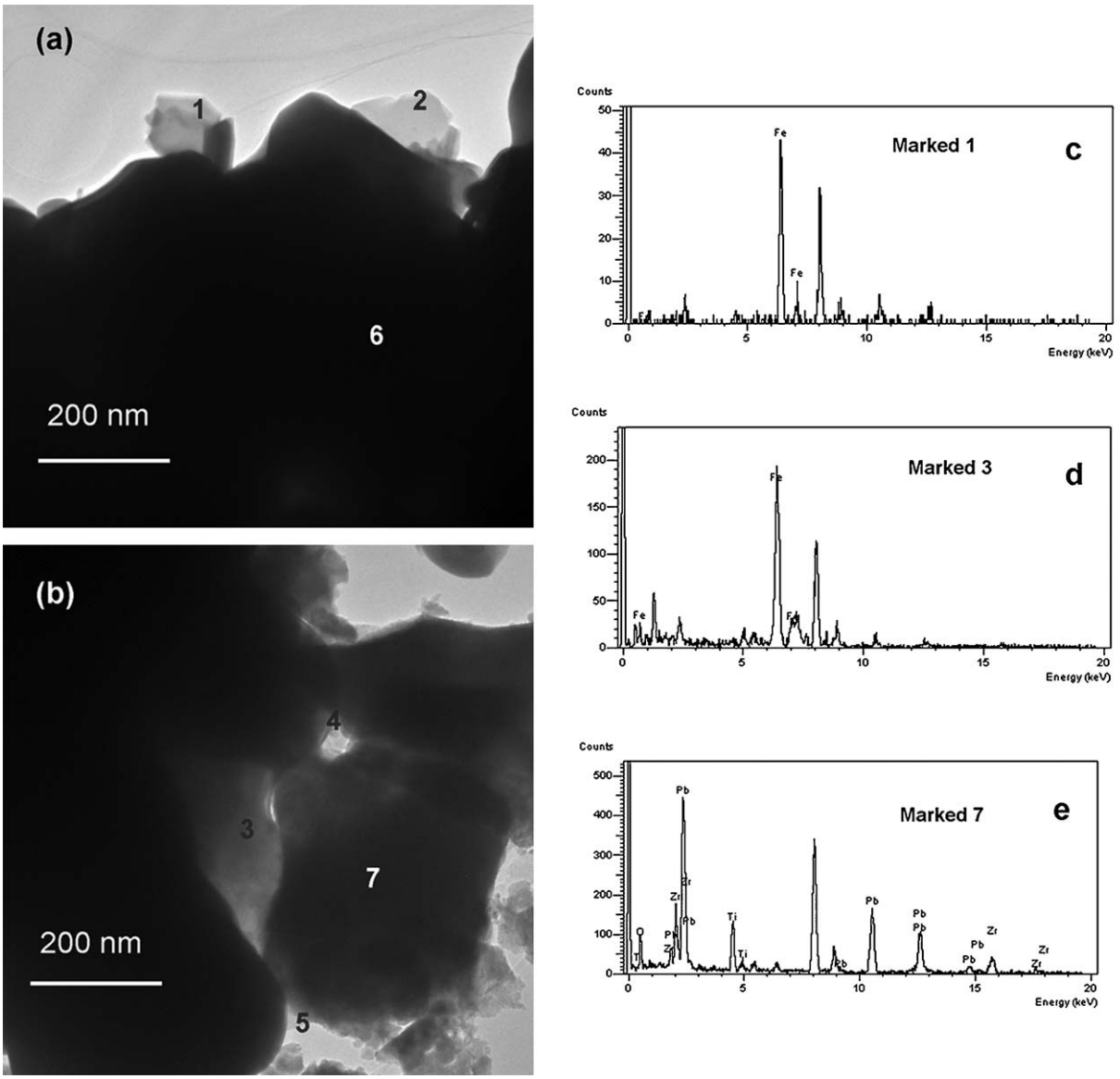

Fig. 4. (a) TEM images of the interlayer corresponding to Fig. 3(c). EDS spectra in Fig. 4(c)–(e) respectively correspond to the analytical points marked "1–7" in Fig. 4(a) and (b).

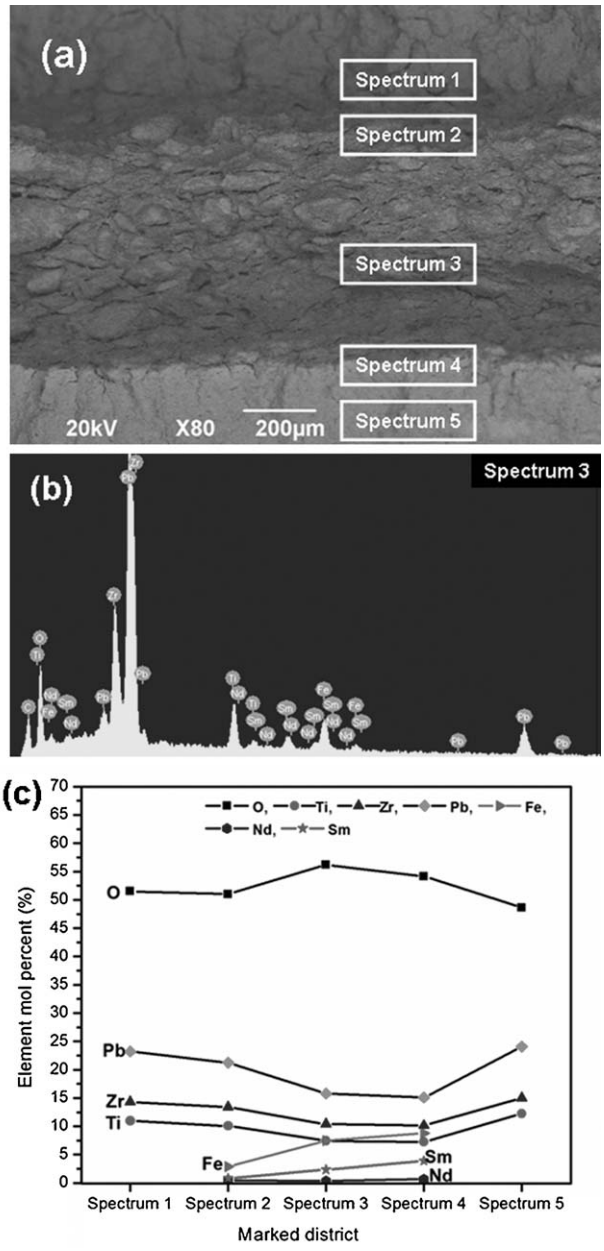

Fig. 5. (a) Typical backscattering of the fractured surface of the composite with 5 wt% MS content, together with (b), and (c) elemental distribution analysis of the marked districts.

coexistence of the ferromagnetic and ferroelectric phases simultaneously.

3.2. Magnetic properties

Fig. 6(a) shows the room temperature magnetic hysteresis loops of the 1–10 wt% composites sintered at 900 °C for 4 h in argon, and (b) the hysteresis loop for the typical 3 wt% sample coated by silver electrode, along with their saturation magnetizations and coercive fields in Fig. 6(c).

In Fig. 6(a), all the composites exhibit typical ferromagnetic hysteresis loops (the enlarged loop of 1 wt% sample is shown in the inset), as well as remanent magnetization, thus indicating the presence of a spontaneous magnetic property. The M–H loops prove and confirm the existence of $Sm_{0.88}Nd_{0.12}Fe_{1.93}$ phase in all the three-ply structured ceramic composites. For example, in the 5 wt% composite the saturation and remanent magnetizations are found to be 2.1407 emu/g and 1.0085 emu/g, respectively. To confirm that ferromagnetism exists in the composite coated with the silver electrode at 600 °C at air, in Fig. 6(b), it is clear that the M–H hysteresis loop of the typical 3 wt% sample also is observed in the composite. However, compared with the counterpart of the composite without the electrode, the remanent and saturation magnetization is a little bit lower, the reason is uncertain and will be further studied in future work. But the present work has proved that the novel three-ply structured composite indeed can be cofired in air or argon in spite of the composites containing a metal alloy powder.

From Fig. 6(c), it is clear that the remanent and saturation magnetizations both increase with the increase in $Sm_{0.88}Nd_{0.12}Fe_{1.93}$ content. This indicates that the spontaneous magnetization of the composites originates from the alignment of ionic magnetic moments in domain structures. We also found that the intrinsic coercivity (H_{ci}) increases with increasing $Sm_{0.88}Nd_{0.12}Fe_{1.93}$ content, for instance, in the composite with 3 wt% of $Sm_{0.88}Nd_{0.12}Fe_{1.93}$, the H_{ci} is about 1376 Oe, while for the sample with 10 wt% of content, the H_{ci} is round 1990 Oe. It reveals that the maximum energy product [$(BH)_{max}$, B denotes magnetic induction, and H denotes magnetic field intensity] can be obtained due to the finer-grained microstructure in the $Sm_{0.88}Nd_{0.12}Fe_{1.93}$ particles by the high-energy ball milling,[30] and the ferromagnetic properties of $Sm_{0.88}Nd_{0.12}Fe_{1.93}$ phase can be retained, which is an important advantage of the composites.

3.3. Ferroelectric properties

Fig. 7(a)–(d) show the polarization-field hysteresis loops of the composite ceramics containing (a) 1 wt%, (b) 3 wt%, (c) 5 wt%, and (d) 7 wt% of $Sm_{0.88}Nd_{0.12}Fe_{1.93}$ content at the frequency of 100 Hz, respectively. In Fig. 7(a) and (b), apparent P–E loops were observed indicating that the composites are ferroelectric. For the1 wt% and 3 wt% composites, the remanent polarization (P_r) is 1.67 μC/cm^2, and 0.78 μC/cm^2, respectively, while the coercive field (E_c) is 0.81 kV/mm and 0.99 kV/mm, respectively. However, with increasing $Sm_{0.88}Nd_{0.12}Fe_{1.93}$ content, the conduction contribution increases, the shape of the ferroelectric hysteresis loops [in Fig. 7(c) and (d)] becomes elliptical. [31] The coercive field (E_c) and saturation polarization (P_s) are affected and enhanced in the course of the dielectric polarization process. However, these results confirm that the composites possess ferroelectric properties.

Also, it is seen in Fig. 7 that the polarization hysteresis loops are slightly shifted to the right, which is presumably attributed to the space charge at low-frequency due to the characteristics of three-ply structured composite, arising from the insulating layers (PZT) and the interlayer consisting of conducting grains of ($Sm_{0.88}Nd_{0.12}Fe_{1.93}$) separated by insulating intergrain barriers (PZT), some related results will be discussed in more details elsewhere.

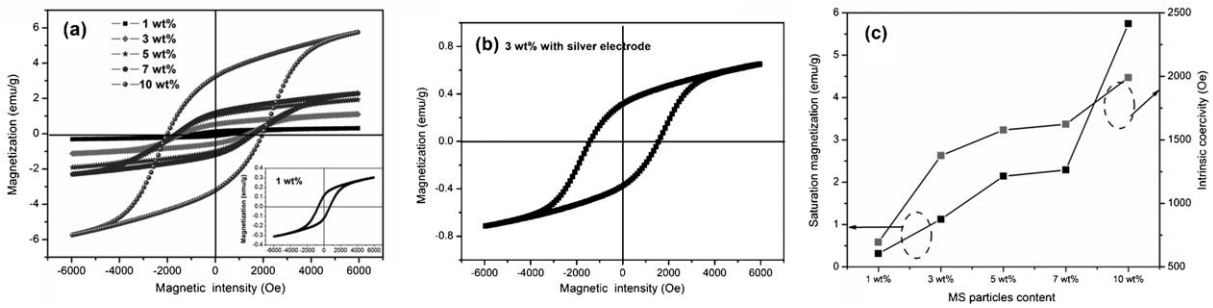

Fig. 6. (a) Room-temperature magnetic-hysteresis loops of composites with various MS contents sintered at 900 °C in argon, (b) the magnetic-hysteresis loop of a typical composite with 3 wt% MS content coated by silver electrode in air, together with (c) their saturation magnetizations and coercive fields.

3.4. Dielectric properties and DC resistivity

The variations of dielectric constant and loss tangent with frequency are shown in Fig. 8(a) and (b), together with (c) DC resistivity for the composites with the $Sm_{0.88}Nd_{0.12}Fe_{1.93}$ content of 1–10 wt%, respectively, at room temperature, a set of equivalent LC circuit is shown inside Fig. 8(c). In Fig. 8(a), with increasing MS content, the dielectric constant decreases except for the 10 wt% composite. For instance, at 100 Hz, in the 1 wt% composite, the dielectric constant is ~333, and the 7 wt%

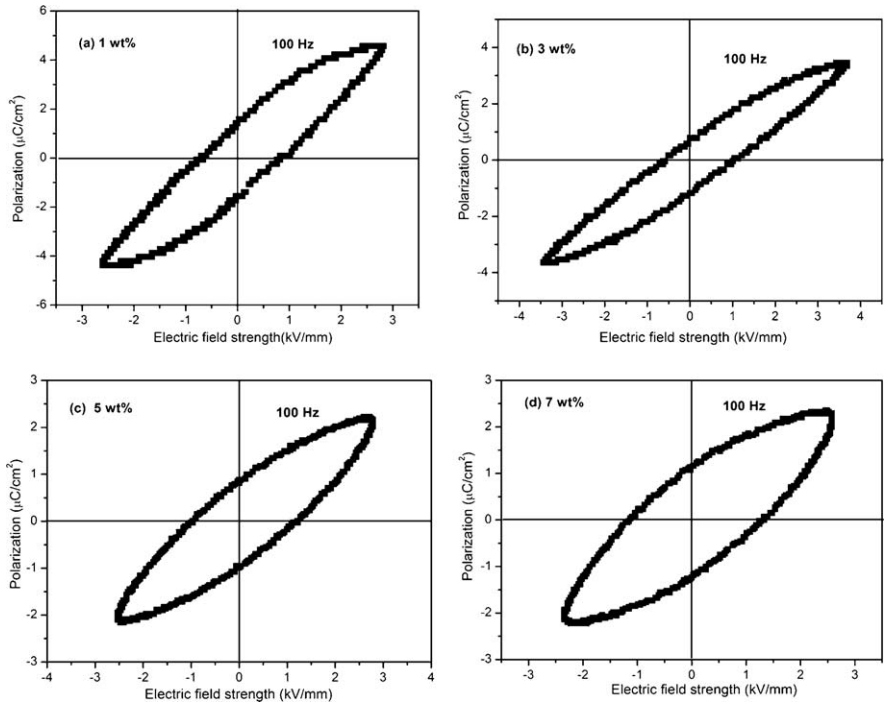

Fig. 7. Polarization-field hysteresis loops of the composite ceramics containing (a) 1 wt%, (b) 3 wt%, (c) 5 wt%, and (d) 7 wt% MS contents at the frequency of 100 Hz, respectively.

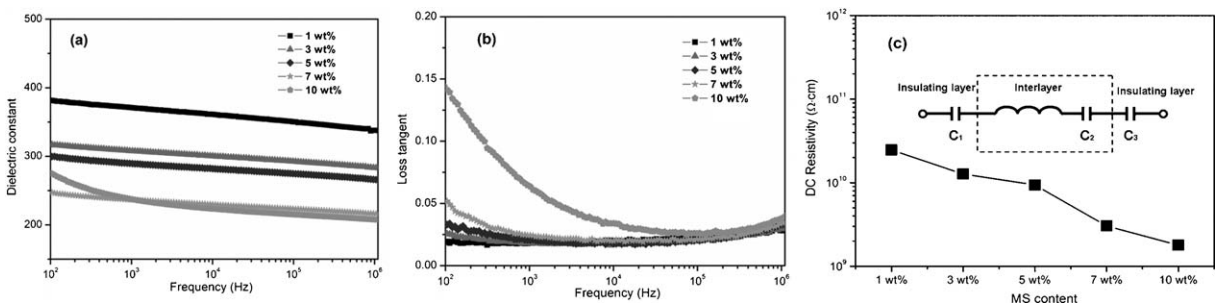

Fig. 8. Frequency dependence of dielectric constant (a), loss tangent (b) respectively, together with (c) the DC resistivity as a function of the MS content, inside a set of equivalent LC circuit.

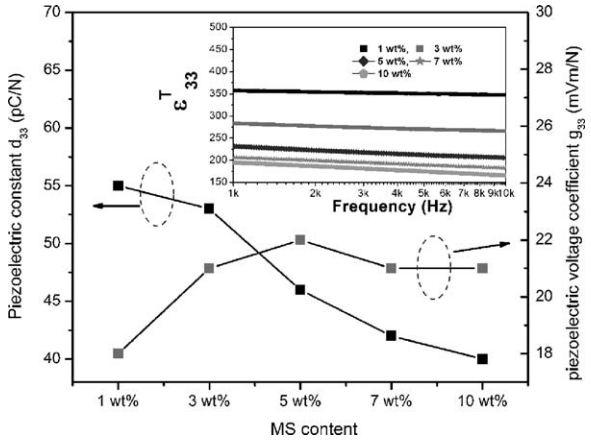

Fig. 9. Piezoelectric characteristics of the three-ply structured composites as a function of wt% of MS content, besides the relative permittivity ε^T_{33} between 1 kHz and 10 kHz at room temperature shown in the inset.

composite has a dielectric constant of ~247. The fall in dielectric constant is attributed to the fact that the interlayer in which ferroelectric regions (PZT) are surrounded by nonferroelectric regions ($Sm_{0.88}Nd_{0.12}Fe_{1.93}$) similar to the relaxor ferroelectric materials. At lower frequencies (100 Hz), a slightly larger value of dielectric constant is observed attributed to the features of the new structure as mentioned above, and the dielectric dispersion is due to interfacial polarization in agreement with Koop's phenomenological theory.[32] The variation of loss tangent with frequency is shown in Fig. 8(b). Similarly, at lower frequencies, with increasing MS content, the loss tangent increases. For instance, at 100 Hz, in the 1 wt% and 7 wt% composite, loss tangent is ~0.016, and ~0.05, respectively; while in the 10 wt% composite, loss tangent is ~0.14 at 100 Hz. Loss tangent is proportional to the 'loss' of energy from the applied field on the sample (in fact this energy is dissipated into heat) and therefore denoted as dielectric loss. At low frequency, space charge polarization and AC conductivity (electrical leakage) contribute to the dielectric loss. And at higher frequencies, the losses are reduced and the dipoles contributed to the polarization. In Fig. 8(c), the DC resistivity as high as 10^9–10^{10} Ω.cm was observed indicating a full dense three-ply-structured composites is a nonconductive materials. It is noted the DC resistivity only decreases slightly (by a factor of 10) as the MS content increases from 2.4 to 21.73 wt% in the interlayer, which is due to the new three-ply structure. Because the result can be approximately described by a set of LC equivalent circuit that consists of one self-inductance, three capacitors (C_1, C_2, and C_3) in series ($Q_1 = Q_2 = Q_3$, where Q is charge), as shown in the inset of Fig. 8(c). With an increase in the conductive phase, the interlayer can be regarded as a conductive layer with low resistivity; however, there is a slight impact on the insulating layers (that is, C_1 and C_3), thus the leakage current depends mainly on the insulating layers. This is one significant feature of the new structure composites. The critical volume fraction, i.e. percolation threshold limits (causing the dynamic properties variance such as low resistivity which restricts with the application in metal-insulator composite materials) is less than that of other materials [33] (the look-alike phenomena were reported in Yoon et al's [34]).

3.5. Piezoelectric behavior

All the samples are electrically polarized in silicone oil under a poling field of 3–4 kV/mm and at temperature around 150–180 °C for 30 min. The piezoelectric characteristics were measured 24 h after poling. The piezoelectric characteristics of the composites containing 1, 3, 5, 7 and 10 wt% of $Sm_{0.88}Nd_{0.12}Fe_{1.93}$ content are investigated briefly in this work and shown in Fig. 9, together with the room-temperature relative permittivity ε^T_{33} at 1–10 kHz shown in the inset. Interestingly, the piezoelectric constant d_{33} (piezoelectric charge coefficient) is between 55 and 40 pC/N, and the k_p (planar electromechanical coupling factor) by means of the standard resonance method [35] using the same impedance analyzer is between 0.14 and 0.18. As shown in the inset, the relative permittivity ε^T_{33} is almost constant between 1 kHz and 10 kHz, the g_{33} (piezoelectric voltage coefficient, ε^T_{33} at 1 kHz) varies slightly from 18 to 22 mVm/N for composites with different amounts of highly conductive phase ($Sm_{0.88}Nd_{0.12}Fe_{1.93}$). With increasing in the ferromagnetic content, piezoelectricity of the composites depends mainly on the insulating layer, which is one of the advantages of using the novel structure in the multiferroic composite materials. This implies that desired piezoelectricity of the composites can be obtained by adjusting the piezoelectric properties of the insulating layers via a simple, easy, and flexible way.

4. Conclusions

Multiferroic ceramic composites combining $Sm_{0.88}Nd_{0.12}Fe_{1.93}$ and PZT with a novel three-ply structure have been successfully synthesized by conventional ceramics process. TEM images show homogeneity of the metal particle dispersion and a good interfacial contact between bi-phase powders in the composite. The coexistence of ferromagnetism and ferroelectricity has been confirmed by means of P–E and M–H curve measurements at room temperature. The breakthrough of the novel structure in term of the described above includes:

(1) Cofiring can avoid the polymer binder used in composite materials, and the three-structures (three layers: insulting layers and interlayer) can be flexibly adjusted to meet the various design requirements, such as capacitance, piezoelectricity, or ferromagnetism and so on.
(2) Low temperature sintering, ensuring a highly dense, smooth and flat insulating layer, can mitigate the element and chemicals evaporation, also suppress the diffusion of the highly conductive phase and prevent interfacial diffusion or chemical reaction between the constituents in the composites. At the same time, the low temperature sintering can ease the trouble of thermal expansion during the sintering course, or cofiring is an impossible mission in preparation of the composites consisting of the highly conductive phase (such

as $Sm_{0.88}Nd_{0.12}Fe_{1.93}$) and insulator phase (i.e. PZT). The success is attributed to the modified hybrid process.

(3) Low temperature silver paste can be coated on the two sides of the composite and fired-on in air. Poling can be acted at high electric field strength at high temperature. This implies that the three-ply structured composite can be heated under ambient air condition without having effect on the magnetic properties of the magnetostrictive phase.

(4) The DC resistivity as high as 10^9–10^{10} Ω.cm was observed despite the composites have a high wt% of conductive alloy content, the piezoelectric properties mainly depend on the properties of the insulating layers. Thus, the novel structure provides a great room for the composite to be tailored by adjusting the piezoelectric properties of the insulating layers via a simple, easy, and flexible way.

Acknowledgements

This work was supported by the Research Grants Council of the HKSAR Government under Grant No. PolyU 5266/08E, the Hong Kong Polytechnic University Grant Nos. 4-ZZ7T and 1-ZV7P, and NSFC/RGC Project No. N_PolyU 501/08.

References

1. Schmid H. Multi-ferroic magnetoelectrics. *Ferroelectrics* 1994;**162**:317–38.
2. Kanai T, Ohkoshi S, Nakajima A, Watanabe T, Hashimoto K. A ferroelectric ferromagnet composed of $(PLZT)_x(BiFeO_3)_{1-x}$ solid solution. *Adv Mater* 2001;**13**:487–9.
3. Qi XW, Zhou J, Yue ZX, Gui ZL, Li LT, Buddhudu S. A ferroelectric ferromagnetic composite materials with significant permeability and permittivity. *Adv Funct Mater* 2004;**14**:920–6.
4. Lin Y, Cai N, Zhai J, Liu G, Nan CW. Giant magnetoelectric effect in multiferroic laminated composites. *Phys Rev B* 2005;**72**:012405.
5. Park CS, Ahn CW, Ryu J, Yoon WH, Park DS, Kim HE, Priya S. Design and characterization of broadband magnetoelectric sensor. *J Appl Phys* 2009;**105**:094111.
6. Wang KF, Liu JM, Ren ZF. Multiferroicity: the coupling between magnetic and polarization orders. *Adv Phys* 2009;**58**:321–448.
7. Gao F, Chen XY, Yin KB, Dong S, Ren ZF, Yuan F, Yu T, Zou ZG, Liu JM. Visible-light photocatalytic properties of weak magnetic $BiFeO_3$ nanoparticles. *Adv Mater* 2007;**19**:2889–92.
8. Yuan GL, Or SW, Chan WHL. Structural transformation and ferroelectric–paraelectric phase transition in $Bi_{1-x}La_xFeO_3$ ($x = 0$–0.25) multiferroic ceramics. *J Phys D: Appl Phys* 2007;**40**:1196–200.
9. Spaldin NA, Fiebig M. The renaissance of magnetoelectric multiferroics. *Science* 2005;**309**:391–2.
10. O'Dell TH. *The electrodynamics of magneto-electric media*. Amsterdam: North-Holland; 1970.
11. Li TL, Study of magnetoelectric composites for senor and transducer applications. Ph.D dissertation, 2005.
12. Folen VJ, Rado GT, Stalder EW. Anisotropy of the magnetoelectric effect in Cr_2O_3. *Phys Rev Lett* 1961;**6**:607–8.
13. Suchetelene JV. Product properties: a new application of composite materials. *Philips Res Rep* 1972;**27**:28–37.
14. Chashin DV, Fetisov YK, Kamentsev KE, Srinivasan G. Resonance magnetoelectric interactions due to bending modes in a nickel-lead zirconate titanate bilayer. *Appl Phys Lett* 2008;**92**:102511.
15. Ryu J, Priya S, Uchino K, Kim HE. Magnetoelectric effect in composites of magnetostrictive and piezoelectric materials. *J Electroceram* 2002;**8**:107–19.
16. Wang YJ, Or SW, Chan WHL, Zhao XY, Luo HS. Enhanced magnetoelectric effect in longitudinal–transverse mode Terfenol-D/$Pb(Mg_{1/3}Nb_{2/3})O_3$–$PbTiO_3$ laminate composites with optimal crystal cut. *J Appl Phys* 2008;**103**:124511.
17. Wang YJ, Or SW, Chan WHL, Zhao XY, Luo HS. Magnetoelectric effect from mechanically mediated torsional magnetic force effect in NdFeB magnets and shear piezoelectric effect in $0.7Pb(Mg_{1/3}Nb_{2/3})O_3$–$0.3PbTiO_3$ single crystal. *Appl Phys Lett* 2008;**92**:123510.
18. Wang YJ, Wang FF, Or SW, Chan WHL, Zhao XY, Luo HS. Giant sharp converse magnetoelectric effect from the combination of a piezoelectric transformer with a piezoelectric/magnetostrictive laminated composite. *Appl Phys Lett* 2008;**93**:113503.
19. Li YJ, Chen XM, Lin YQ, Tang YH. Magnetoelectric effect of $Ni_{0.8}Zn_{0.2}Fe_2O_4/Sr_{0.5}Ba_{0.5}Nb_2O_6$ composites. *J Eur Ceram Soc* 2006;**26**:2839–44.
20. Zhang HF, Or SW, Chan WHL. Multiferroic properties of $Ni_{0.5}Zn_{0.5}Fe_2O_4$–$Pb(Zr_{0.53}Ti_{0.47})O_3$ ceramic composites. *J Appl Phys* 2008;**104**:104109.
21. Zhang HF, Or SW, Chan WHL. Fine-grained multiferroic $BaTiO_3/(Ni_{0.5}Zn_{0.5})Fe_2O_4$ composite ceramics synthesized by novel powder-in-sol precursor hybrid processing route. *Mater Res Bull* 2009;**44**:1339–46.
22. Ma J, Shi Z, Nan CW. Magnetoelectric properties of composites of single Pb(Zr Ti)O_3 rods and Terfenol-D/Epoxy with a single-period of 1–3-Type structure. *Adv Mater* 2007;**19**:2571–3.
23. Eerenstein W, Mathur ND, Scott JF. Multiferroic and magnetoelectric materials. *Nature* 2006;**442**:759–65.
24. Petrov VM, Bichurin MI, Modeling of magnetoelectric effects in ferromagnetic/piezoelectric bulk composites. Magnetoelectric Interaction Phenomena in Crystals, Proceedings of the NATO ARW on Magnetoelectric Interaction Phenomena in Crystals, Sudak, Ukraine from 21 to 24 September 2003. Manfred F, Victor VE, and Irina EC, (Eds.); 2004, 65–70.
25. Babu VH, Markandeyulu G, Subrahmanyam A. Giant magnetostriction in $Sm_{1-x}Nd_xFe_{1.93}$ compounds. *Appl Phys Lett* 2007;**90**:252513.
26. Muñoz JE, Cervantes J, Esparza R, Rosas G. Iron nanoparticles produced by high-energy ball milling. *J Nanopart Res* 2007;**9**:945–50.
27. Zhang HF, Or SW, Chan WHL. Synthesis of fine-crystalline $Ba_{0.6}Sr_{0.4}TiO_3$–MgO ceramics by novel hybrid processing route. *J Phys Chem Solids* 2009;**70**:1218–22.
28. Zhang HF, Yao X, Zhang LY. Microstructure and dielectric properties of barium strontium titanate thick films and ceramics with a concrete-like structure. *J Am Ceram Soc* 2007;**90**:2333–9.
29. Hwang HJ, Nagai T, Ohji T, Sando M, Toriyama M. Curie temperature anomaly in lead zirconate titanate/silver composites. *J Am Ceram Soc* 1998;**81**:709–12.
30. Wang KY, Wang YZ, Yin L, Song L, Rao XL, Liu GC, Hu BP. $Sm_2Fe_{17}N_y$ powder with high coercivity preprared by high energy ball milling. *Solid State Commun* 1993;**88**:521–3.
31. Scott JF. Ferroelectrics go bananas. *J Phys Condens Matter* 2008;**20**:1–2.
32. Koops CG. On the dispersion of resistivity and dielectric constant of some semiconductors at audiofrequencies. *Phys Rev* 1951;**83**:121–4.
33. Pecharromán C, Moya JS. Experimental evidence of a giant capacitance in insulator-conductor composites at the percolation threshold. *Adv Mater* 2000;**12**:294–7.
34. Yoon CB, Lee SH, Lee SM, Kim HE. Co-firing of PZN-PZT flextensional actuators. *J Am Ceram Soc* 2004;**87**:1663–8.
35. IEEE Standard on Piezoelectricity ANSI/IEEE Standard 176–1978, Institute of Electrical and Electronic Engineers, New York, 1978.